Available online at www.sciencedirect.com
SCIENCE DIRECT®
Journal of Sound and Vibration 260 (2003) 117–139
JOURNAL OF SOUND AND VIBRATION
www.elsevier.com/locate/jsvi

Theories and experiments on the stiffening effect of high-frequency excitation for continuous elastic systems

J.J. Thomsen*

Department of Mechanical Engineering, Solid Mechanics, Technical University of Denmark, Building 404, DK-2800 Lyngby, Denmark

Received 29 October 2001; accepted 7 March 2002

Abstract

One effect of strong mechanical high-frequency excitation may be to apparently "stiffen" a structure, a well-described phenomenon for discrete systems. The present study provides theoretical and experimental results on this effect for continuous elastic structures. A laboratory experiment is set up for demonstrating and measuring the stiffening effect in a simple setting, in the form of a horizontal piano string subjected to longitudinal high-frequency excitation at the clamped base and free at the other end. A simplest possible theoretical model is set up and analyzed using a hierarchy of three approximating theories, each providing valuable insight. One of these is capable of predicting the vertical string lift due to stiffening in terms of simple expressions, with results that agree very well with experimental measurements for a wide range of conditions. It appears that resonance effects cannot be ignored, as was done in a few related studies—unless the system has very low modal density or heavy damping; thus first-order consideration to resonance effects is included. Using the specific example with experimental support to put confidence on the proposed theory, expressions for predicting the stiffening effect for a more general class of continuous systems in differential operator form are also provided.
© 2002 Elsevier Science Ltd. All rights reserved.

1. Introduction

This work concerns setting up and testing analytical expressions for the stiffening effect of strong high-frequency (HF) excitation for continuous elastic systems. This involves presenting the phenomenon in a simple physical setting, setting up a laboratory experiment that allows visual demonstration and accurate measurements, providing a simplest possible theory that correlates well with experiments, and generalizing that theory to a wider class of elastic systems. The study is

*Tel.: +45-45-25-42-50; fax: +45-45-93-14-75.
E-mail address: jjt@mek.dtu.dk (J.J. Thomsen).

0022-460X/03/$ - see front matter © 2002 Elsevier Science Ltd. All rights reserved.
PII: S0022-460X(02)00916-1

believed to be the first providing experimental results and theoretical predictions that agree quantitatively on the stiffening effect for a continuous elastic system.

The laboratory experiment involves a clamped-free piano string, horizontally aligned and subjected to longitudinal high-frequency excitation at the clamped end. Gravity causes the string to bend downwards, while the HF excitation generally causes it to stiffen and thus to straighten somewhat. Measuring the lift of the string then quantifies the stiffening effect. A simple linear beam model is set up, and analyzed using three theories: A simple one giving insight but poor accuracy, a detailed one giving good accuracy but little insight, and a compromise capable of predicting the average tip lift in good quantitative agreement with experimental results for a wide range of conditions, except at sharp resonance. It appears that resonance effects cannot be ignored, as was done in the few related studies, since the modal density is high and damping is weak: Even the flattest parts of the frequency response is affected by neighboring resonances. Thus the theoretical predictions include first-order consideration to resonance effects. Using the specific example with experimental support to put confidence on the proposed theory, expressions for predicting the stiffening effect for a more general class of continuous systems in differential operator form are also provided and exemplified.

Several non-trivial effects of strong HF excitation has been described, e.g., in Refs. [1–5], among them the stiffening effect of present concern. One well-known manifestation of it is the stabilization of the upper equilibrium position of a pendulum on a rapidly vibrating support, as described already by Stephenson [6,7], Hirsch [8], and Kapitza [9]. Similar effects may occur for systems with multiple degrees of freedom, e.g., double- or n-link pendulums [1,10–14], and as well for continuous structures such as strings, rods, beams, membranes, plates and shells.

For continuous systems Chelomei, in a popular exposition [15], demonstrated experimentally how HF axial excitation could increase the buckling stability of a pinned–pinned column. The change of stability can be seen as a consequence of a change in effective stiffness, i.e., stiffness "on the average", as predicted much earlier by Chelomei [16] using a simple linear model. Later Jensen [17] presented an extended theoretical model of this system, paying consideration to non-linear effects and imperfections, and provided a thorough analysis of how equilibriums of the column emerge and disappear and changes stability as parameters of the HF excitation is varied. In Ref. [18] the theoretical predictions were supplied with predictions for the corresponding change in effective natural frequencies; these were tested experimentally, giving reasonable agreement at least qualitatively. However, there were also significant discrepancies, and it was not clear which unmodelled features should be included in the theory to reduce these.

Other investigations with experimental support seem rare: Feuer and Levine [10] studied the stabilizing effect of applying HF excitation to a clamped–free flexible beam; the beam was modelled as an n-link mechanism, and laboratory experiments with a 2-link beam showed a clear stiffening effect of the excitation. Also, Champneys and Fraser [19,20] presented a theoretical and numerical analysis of the stabilizing effect of HF excitation for a vertical clamped–free beam (a phenomenon that Ref. [21] refers to as "not quite the Indian rope trick"). The motivation of the study was to explain experiments performed by Mullin and described in Ref. [21] using pieces of curtain wire (see also Refs. [12,22]); however, the authors concluded that close quantitative agreement between theory and experiment could not be found.

Previous theoretical predictions for the stiffening effect assumes strictly non-resonant excitation: Tcherniak [23] analyzed a pinned–pinned beam, and showed how a combination of

axial point loads and distributed loads of high frequency may be used to change natural frequencies and mode shapes of the beam. The assumption of non-resonant excitation is shown to be theoretically fulfilled if the damping is internal (i.e., is proportional to the rate of change of bending moment). Then all modes above a certain frequency are over-damped, and excitations above this frequency cannot excite (first-order) resonances. Also, Hansen [24] used theoretical and numerical analysis to predict an increase of the natural frequencies of a spinning flexible disk subject to a small but rapid pulsating overlay in rotation speed. Again the analysis assumes the pulsating overlay to be non-resonant to the disk system, and the agreement with numerical analysis is good only when this is fulfilled. Also Zak [25], considering general elastic continua in HF excitation fields, showed that stiffening occurs in the direction of the wave vector and provided expressions for the effective Young's modulus, again with resonance effects neglected.

The present study attempts to set up a laboratory experiment for illustrating and measuring the phenomenon for a simple string case (Section 2), set up approximate analytical expressions for predicting measurable quantities of the phenomena for that case with good accuracy (Section 3), test these expressions against numerical simulation and experimental measurements (Section 4), and on that basis suggest similar theoretical expressions for a generalized class of HF excited elastic systems of differential operator form (Section 4).

2. Example system: flexible beam with HF base excitation

2.1. The system and the phenomenon

The prime phenomenon under consideration is the apparent change in stiffness that may accompany strong HF excitation. This change in turn affects measurable quantities such as deformations under static and dynamic loading, natural frequencies, and buckling stability. *Deformation* is chosen as the quantity to be measured experimentally and predicted theoretically, since it can be measured rather easily (by contrast to buckling stability) and even be judged visually (as opposed to natural frequencies).

Fig. 1 shows a doubly exposed photo of a thin horizontal piano string exposed to gravity (lower string image), and to additional horizontal base vibrations having small displacement amplitude, but high frequency and thus significant acceleration amplitude (upper image). As is evident, the exciting vibrations cause the string to vibrate transversely (image slightly blurred), and to lift off noticeably from the static equilibrium. Filtering or averaging out the small overlay of HF excitation, an observer perceives the lift as an increase in the bending stiffness of the string, since there is no change in (average) external loading.

The string in Fig. 1 was used only for visual demonstrations. To better utilize the measurement range of the available equipment, a much stiffer string showing consequently smaller deformations was used for recorded measurements, as described next.

2.2. Experimental setup and procedure

All recorded measurements were obtained for a 1 mm diameter piano string of length 550 mm, density 7819 kg/m (weight and dimensions measured), Young's modulus 195 GPa (estimated by

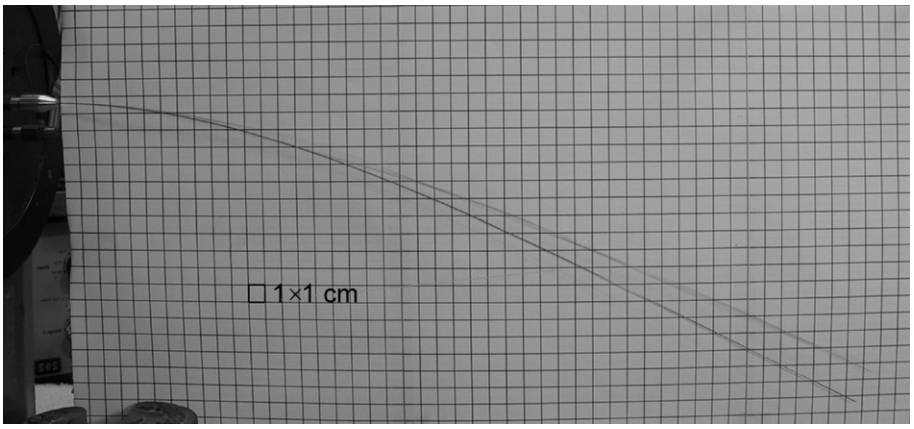

Fig. 1. String $\varnothing 0.5 \times 500$ mm excited by horizontal vibrations at the base. Two images overlaid: One with gravity as the only excitation (lower string image), and one with the base vibrating at 62 Hz and 3.3 mm displacement, 500 m/s^2 acceleration amplitude (upper image). The string tip is seen to lift about 2 cm. Camera shutter speed was $\frac{1}{50}$ s, so the blurred image of the upper string reflects positions traced during a little more than a full vibration cycle.

Table 1
Measured natural frequencies f_i, damping ratios ζ_i, and relative deviation between measured and theoretically predicted (Bernoulli–Euler) natural frequencies $\Delta f_i/f_i$ for the $\varnothing 1 \times 550$ mm clamped-free piano string

i	1	2	3	4	5	6
f_i (Hz)	2.4	14.6	40.4	79.1	131.0	195.6
ζ_i (%)	4.5	0.3	0.3	0.06	0.05	0.05
$\Delta f_i/f_i$ (%)	3.9	0.9	−0.3	−0.4	−0.21	−0.3

fitting to six lowest measured natural frequencies, as obtained using measured frequency responses from pseudo-random excitation and B&K PULSE software), and lowest natural frequencies and estimated modal damping as given in Table 1.

Fig. 2 sketches the setup. The string was horizontally clamped by a rigid stud to a horizontally aligned vibration exciter. The exciter delivers vibrations of adjustable acceleration amplitude and frequency, quantities that were measured using an accelerometer mounted at the shaker base. Motions of the string tip were measured using an optical displacement follower that automatically tracks vertical movements of a horizontal black/white contrast on a small piece of paper glued to the tip. For the actual setup the accuracy of tracker readings was better than 0.1 mm within the measurement range 0–10 mm. The tracker output signal was fed to a digital signal analyzer, where it could be displayed, recorded, and analyzed along with the accelerometer signal from the shaker, in the time or frequency domain.

Calibration of the setup was performed before each measurement series, using a dedicated calibrator for the accelerometer, and a micrometer for the optical tracker. The tracker offset was then adjusted to produce zero output with the string in static equilibrium. The latter part of the calibration was repeated after any event that could permanently disturb the static equilibrium,

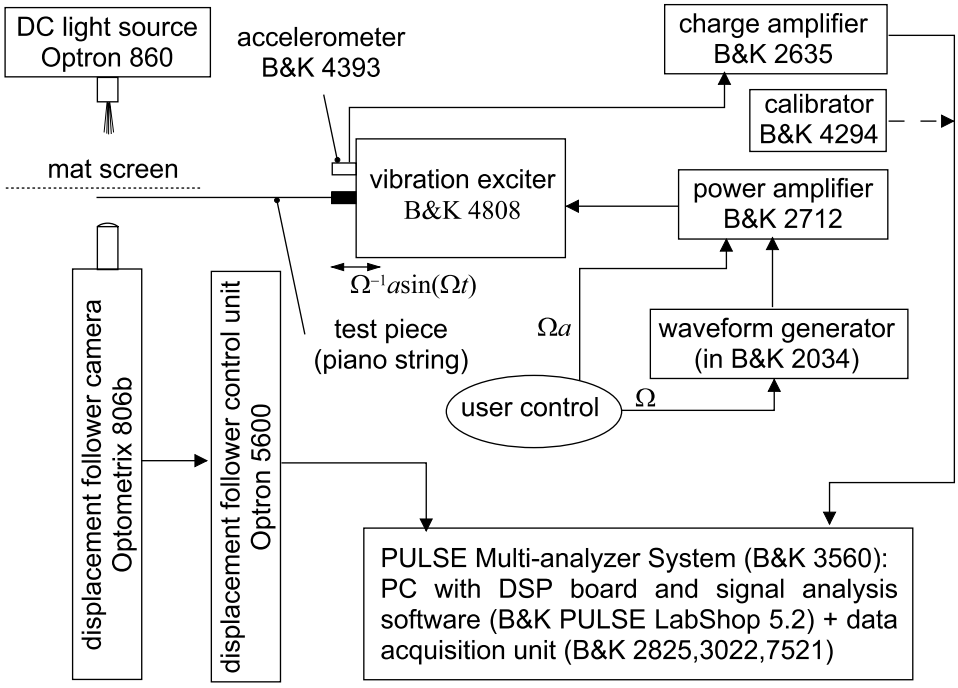

Fig. 2. Experimental setup for measuring base acceleration, base frequency, and tip lift for a clamped-free piano string.

e.g., after violent resonant vibrations. Good reproducibility was observed for all measurements and phenomena. Only stationary outputs were recorded, requiring typically 1/2–2 min of waiting for transients of this lightly damped system to decay to an acceptable level.

Fig. 3 shows a typical time series record, along with definitions of quantities that will be referred to in the following: The *acceleration amplitude* Ωa, the stationary mean *tip lift* $\Delta u_0^*(l)$, and the *tip amplitude* $\hat{u}^*(l)$. As appears the string oscillates in synchrony with the excitation, in this case with a tip lift of about 1.2 mm and amplitude of about 0.4 mm. Analyzing such time series as the two control parameters (base frequency Ω and acceleration Ωa) are varied quasi-statically, one obtains data for *frequency response* or *acceleration response* diagrams, as will be presented in Section 4.

3. Theoretical model and predictions

The aim here is to set up the simplest possible model capable of reproducing the experimental observations with good accuracy. The model is then analyzed using a hierarchy of three theories: A simple one giving insight but poor accuracy, a more detailed one giving good accuracy but little insight, and a third that is believed to represent a good compromise.

Fig. 4 shows a physical model of the string system: a clamped–free beam of free length l, with constant mass per unit length ρA and bending stiffness EI. The beam vibrates in a vertical plane with instant configuration $u(x, t)$, in response to external forces from gravity g and time-harmonic

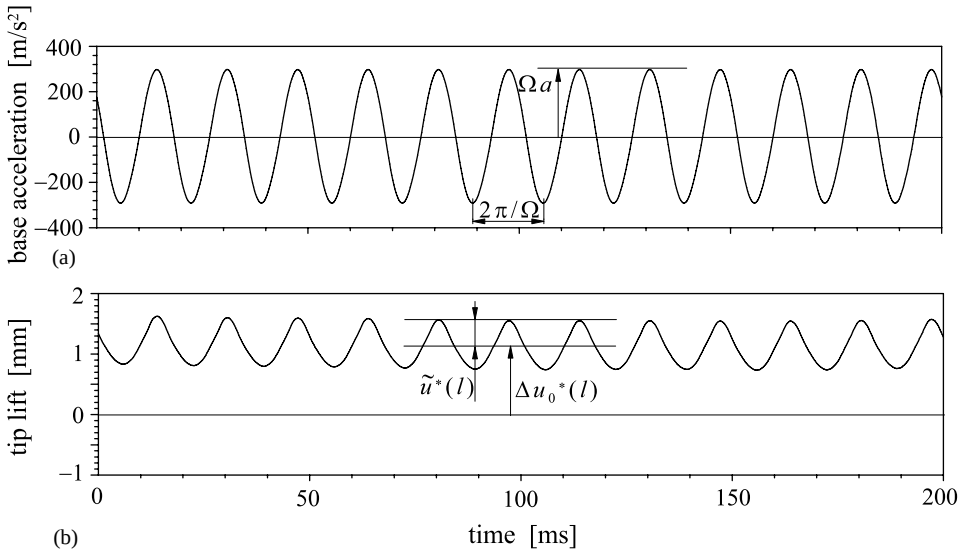

Fig. 3. Sample experimental record of (a) base acceleration and (b) corresponding tip lift for the $\varnothing 1 \times 550$ mm string subjected to 300 m/s^2 base excitation at 60 Hz.

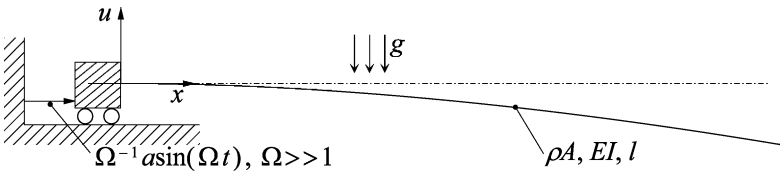

Fig. 4. Physical model of the base excited string.

base excitation. The base excitation has velocity amplitude a and high frequency Ω, so that the displacement amplitude $\Omega^{-1}a$ is small, while the acceleration Ωa is strong. We shall keep referring to the experimental *string* and the corresponding theoretical *beam* model, the latter taking into account the finite bending stiffness of the piano string.

The linearized partial differential equation governing small motions of the beam is obtained by using Newton's second law to express dynamic equilibrium for a differential element of the beam, and employing the usual Bernoulli–Euler assumptions (e.g., see Ref. [26] or most textbooks on basic vibration theory), which yields

$$u_{tt} + cu_t + \omega_0^2 l^4 u_{xxxx} - ((l-x)u_x)_x \Omega a \sin(\Omega t) = -g, \tag{1}$$

$$u(0,t) = u_x(0,t) = u_{xx}(l,t) = u_{xxx}(l,t) = 0, \tag{2}$$

where subscripts x and t denote partial derivatives with respect to space and time, viscous damping with constant coefficient c has been assumed, the quantity $(l-x)u_x\Omega a \sin(\Omega t)$ represents the bending moment per unit length and mass exerted by the moving-base induced inertia forces,

and ω_0 is a characteristic frequency:

$$\omega_0^2 \equiv \frac{EI}{\rho A l^4}. \tag{3}$$

Below predictions are made for the vertical lift of the beam tip due to HF excitation, since this quantity reflects the stiffening effect, and can easily be observed and measured experimentally. Three predictions will be given, each having particular advantages and drawbacks: The *no-resonance prediction* (NRP), the *simulated resonance prediction* (SRP), and the *analytical resonance prediction* (ARP).

3.1. The NRP

This approach is suitable only when the HF excitation is far-from-resonant to the string system, and it cannot easily be generalized to other systems. However, working directly with the partial differential equation of motion, it avoids the errors introduced by discretization, and further reveals quite clearly how the HF excitation effectively corresponds to a spatially varying stiffness distribution.

To analyze Eq. (1) for $\Omega \gg 1$ it is convenient to use the method of direct separation of motions, developed by Blekhman [1] and recently applied for a number of related cases (e.g., Refs. [2,4,5,11]). In this one introduces a fast time τ as a new independent variable, and split the unknown solution into slow and fast components as follows:

$$u(x,t) = u_0(x,t) + \Omega^{-1}u_1(x,t,\tau), \quad \tau \equiv \Omega t, \quad \Omega \gg 1. \tag{4}$$

Here u_0 holds the 'slow' or average motions, and $\Omega^{-1}u_1$ is a rapidly oscillating overlay that has small amplitude, is 2π-periodic in the fast-time τ, and has zero fast-time average:

$$\langle u_1(x,t,\tau)\rangle \equiv \frac{1}{2\pi}\int_0^{2\pi} u_1(x,t,\tau)\,\mathrm{d}\tau = 0, \tag{5}$$

where the slow time t should be considered constant during the (comparably short) time interval of integration. Time derivatives of u transform into partial derivatives with respect to t and τ as follows:

$$u_t = u_{0t} + u_{1\tau} + \Omega^{-1}u_{1t}, \qquad u_{tt} = \Omega u_{1\tau\tau} + u_{0tt} + 2u_{1t\tau} + \Omega^{-1}u_{1tt}. \tag{6}$$

Inserting this and Eq. (4) into Eq. (1) and averaging the result in the sense defined by Eq. (5), one obtains an equation governing the slow motions u_0:

$$u_{0tt} + cu_{0t} + \omega_0^2 l^4 u_{0xxxx} - a((l-x)\langle u_{1x}\sin\tau\rangle)_x = -g, \tag{7}$$

which is similar to Eq. (1) for u (and with identical boundary conditions), though, with the rapidly oscillating term in Eq. (1) replaced by a term representing its *effect* on u_0, on the average.

To obtain an equation for the fast components u_1, one subtracts Eq. (7) from Eq. (1) (with Eqs. (4) and (6) inserted), rearranges, and finds

$$u_{1\tau\tau} = a((l-x)u_{0x})_x \sin\tau + \mathrm{O}(\Omega^{-1}), \tag{8}$$

where $\mathrm{O}(\Omega^{-1})$ represents terms of magnitude order Ω^{-1} and less. A first-order approximate solution for the high-frequency range is thus readily obtained by integration, recalling that u_0 does

not depend on τ, and using condition (5) to eliminate the constants of integration:

$$u_1 = -a((l-x)u_{0x})_x \sin\tau + \mathrm{O}(\Omega^{-1}), \tag{9}$$

This is the *inertial* approximation [1], which neglects any resonant effects of the excitation, if present, and do not generally satisfy the boundary conditions. Despite these deficiencies the inertial approximations has proven useful in a number of applications, since only its integrated effect on u_0, on the average, is of importance. Inserting into Eq. (7) and evaluating the averaging term yields

$$u_{0tt} + cu_{0t} + \omega_0^2 l^4 u_{0xxxx} + \tfrac{1}{2}a^2((l-x)((l-x)u_{0x})_{xx})_x + \mathrm{O}(\Omega^{-1}) = -g, \tag{10}$$

which can be rearranged into the following form:

$$u_{0tt} + cu_{0t} + (\bar{\omega}_0^2(x) l^4 u_{0xx})_{xx} + \mathrm{O}(\Omega^{-1}) = -g, \tag{11}$$

$$\bar{\omega}_0^2(x) \equiv \omega_0^2 + \tfrac{1}{2}(a/l)^2(1-(x/l))^2. \tag{12}$$

Here $\bar{\omega}_0^2(x)$ is seen to represent a distribution of effective bending stiffness (per unit mass) along the string. It is composed of a first term describing the structural or "real" stiffness of the string, and another one equivalencing the average effect of the HF excitation; this part drops of quadratically with x towards the string tip. To an observer filtering out the small overlay of HF excitation, the additional *apparent* stiffness caused by the HF excitation cannot be distinguished from real structural stiffness with the equivalencing distribution.

Stationary solutions $u_0^*(x)$ to the equation of slow motions are found by letting the time-dependent terms in Eq. (11) vanish, and integrating four times to solve the resulting ordinary differential equation for u_0, subject to the boundary conditions (2); this yields

$$u_0^*(x) \equiv \lim_{t\to\infty} u_0 = \begin{cases} \dfrac{-g}{4\omega_0^2}\Big[\mu^{-2}(x/l)^2 + 2\mu^{-3}(1-x/l)(\arctan(\mu) - \arctan(\mu(1-x/l))) \\ \quad +\mu^{-4}\ln\left(\dfrac{1+\mu^2(1-x/l)^2}{1+\mu^2}\right)\Big] + \mathrm{O}(\Omega^{-1}) \quad \text{for } \mu \neq 0, \quad \Omega \gg \omega_0, \\ \dfrac{-g}{24\omega_0^2}[(1-x/l)^4 + 4x/l - 1] \quad \text{for } \mu = 0, \end{cases} \tag{13}$$

where μ is a non-dimensional measure for the velocity amplitude a of the HF excitation:

$$\mu \equiv a/(\sqrt{2}\omega_0 l). \tag{14}$$

The HF excitation changes the (quasi-)equilibrium position of the string, since the stiffness is effectively changed while the loading is not. At $x = l$ this change, which we shall call the *tip lift*, is

$$\Delta u_0^*(l)_{NRP} \equiv u_0^*(l)\big|_{\mu\neq 0} - u_0^*(l)\big|_{\mu=0} = \frac{g}{8\omega_0^2}[1 - 2\mu^{-2}(1-\mu^{-2}\ln(1+\mu^2))] + \mathrm{O}(\Omega^{-1}) \tag{15}$$

while the vibration amplitude at this point, the *tip amplitude*, by Eqs. (4),(9) and (13) becomes

$$\tilde{u}^*(l)_{NRP} \equiv \max(\Omega^{-1}u_1^*) = \frac{\Omega^{-1}g(1-\mu^{-1}\arctan(\mu))}{\sqrt{2}\mu\omega_0} + \mathrm{O}(\Omega^{-2}), \tag{16}$$

where asterisks here and below are used to indicate stationary quantities, and the subscript NRP refers to the no-resonance prediction. In a later section we compare results of the NRP to experimental results and to other predictions.

The bracketed term in Eq. (15) equals the ratio of tip lift (in gravity and HF excitation) to the static tip dip (due to gravity alone). As $\mu \to \infty$ this term approaches unity monotonically from zero, so that the effect of gravity becomes negligible and the string tip lines up with its base. To lift the tip one-tenth of the static dip in gravity requires $\mu \approx 0.41$, while a lift of one half the static dip requires $\mu \approx 1.3$, according to this model.

The NRP in this case provides direct insight into the stiffening effect of HF excitation. However, it is useful only when resonant effect do not occur, as e.g., when the frequency of excitation is in a range where the modal density of the system is very low, or in a range where all modes are over-damped (as with significant internal damping [23]). For the particular string problem it is possible to include first-order consideration to resonant effects, by including the term $\Omega^{-2}\omega_0^2 l^4 u_{1xxxx}$ on the left side of Eq. (8) when solving approximately for u_1; this solution will even satisfy the boundary conditions. However, the final expressions become too complex to provide any meaningful insight, and the approach cannot be generalized very far beyond the present example.

3.2. The SRP

This approach gives results that turn out to match experimental measurements very well, even when the HF excitation is close-to-resonant of the string system. Hence it is used to show that the original model (1)–(2) includes the physical features of primary importance. However, since numerical simulation is required to produce specific predictions for the tip lift, it provides almost no insight into to the principal effect of the HF excitation.

The original partial differential equation of motion (1)–(2) can be solved numerically using e.g., finite element, finite difference, or Galerkin discretization. We use the latter here, since it operates in terms of measurable and interpretable quantities such as natural frequencies and mode shapes, and since the response can be adequately modelled using just a few discretizing functions. Let a solution to Eqs. (1) and (2) be expressed in a series:

$$u(x,t) = \sum_{i=1}^{n} v_i(t)\varphi_i(x), \tag{17}$$

where v_i are unknown time functions, and φ_i are the eigenfunctions for a clamped–free beam:

$$\varphi_i(x) = \cosh\left(\lambda_i \frac{x}{l}\right) - \cos\left(\lambda_i \frac{x}{l}\right) - \frac{(\cosh(\lambda_i) + \cos(\lambda_i))}{(\sinh(\lambda_i) + \sin(\lambda_i))}\left(\sinh\left(\lambda_i \frac{x}{l}\right) - \sin\left(\lambda_i \frac{x}{l}\right)\right), \tag{18}$$

which satisfy the eigenvalue problem $\varphi_{xxxx} = (\lambda/l)^4\varphi$ with boundary conditions as given for u in Eq. (2). Here λ is a solution of the frequency equation $\cos(\lambda)\cosh(\lambda) + 1 = 0$ (e.g., Ref. [26, pp. 61–9], for which the first six approximations are [1.8751041, 4.6940911, 7.8547574, 10.995541, 14.137168, 17.278760]; for $i \geqslant 6$ the deviation from the asymptotic value $\lambda_i \to (2i-1)\pi/2$ is less

than 10^{-7}. The corresponding natural frequencies are

$$\omega_i = \left(\frac{\lambda_i}{l}\right)^2 \sqrt{\frac{EI}{\rho A}} = \lambda_i^2 \omega_0. \tag{19}$$

To perform the Galerkin discretization Eq. (17) is inserted into Eq. (1), multiplied by φ_j, integrated over the beam length, integration by parts employed, the orthogonality properties of φ exploited, and a set of n ordinary differential equations obtained for the modal coefficients $v_i(t)$:

$$v_{itt} + cv_{it} + \omega_i^2 v_i + \sum_{j=1}^{n} \gamma_{ij} v_j \Omega a \sin(\Omega t) = -\beta_i g, \quad i = 1, n, \tag{20}$$

where the modal constants are calculated as follows:

$$\alpha_i \equiv \int_0^l \varphi_i^2 \, \mathrm{d}x; \qquad \beta_i \equiv \alpha_i^{-1} \int_0^l \varphi_i \, \mathrm{d}x, \qquad \gamma_{ij} \equiv \alpha_i^{-1} \int_0^l (l - x) \varphi_{ix} \varphi_{jx} \, \mathrm{d}x. \tag{21}$$

Eq. (20) can be reposed as a set of $2n$ first order differential equations, and solved for $t > 0$ for specific initial conditions and parameters (c, ω_i, Ω, a) by using standard software (DIVPAG from the IMSL Math/Library was used, with an option set to use Gear's BDF method for stiff systems).

Let $v_i^*(t)$ denote a specific stationary solution to Eq. (20), i.e., a numerical solution with initial transients discarded. Then the tip lift becomes, by Eqs. (17) and (20),

$$\begin{aligned} \Delta u_0^*(l)_{SRP} &\equiv (t_2 - t_1)^{-1} \int_{t_1}^{t_2} u^*(l,t)\big|_{a \neq 0} \, \mathrm{d}t - u^*(l,t)\big|_{a=0} \\ &= (t_2 - t_1)^{-1} \sum_{i=1}^{n} \int_{t_1}^{t_2} v_i^*(t) \, \mathrm{d}t \, \varphi_i(l) + g \sum_{i=1}^{n} \beta_i \omega_i^{-2} \, \varphi_i(l), \end{aligned} \tag{22}$$

where the averaging integration is performed numerically for the numerical solution v_i^* over a suitable post-transient time interval $[t_1; t_2]$. The tip amplitude becomes, by Eq. (17),

$$\tilde{u}^*(l)_{SRP} \equiv \frac{1}{2} \sum_{i=1}^{n} \left(\max_{t \in [t_1; t_2]} (v_i^*) - \min_{t \in [t_1; t_2]} (v_i^*) \right) \varphi_i(l), \tag{23}$$

where subscript SRP refers to the simulated resonance prediction. The accuracy of the numerical solution increases with the number n of eigenfunctions included in the expansion. However, since the response is typically dominated by lower modes, good accuracy can usually be attained by including all modes having natural frequencies near to and lower than the frequency Ω of excitation.

3.3. The ARP

The next approach provides analytical predictions in terms of simple functions of natural frequencies and mode shapes. Combining the approaches for the NRP and the SRP described above, it employs Galerkin discretization to obtain approximating ordinary differential equations, which are then solved using the method of direct separation of motions. It provides predictions almost as close to experimental observations as the SRP, except at sharp resonance. And yet it

allows analytical insight and straightforward calculation. Most importantly, the approach can be generalized for a wider class of elastic systems.

It should be stressed that we are concerned with small but rapid vibrations of the system, since only then is it meaningful to consider the average vibration amplitude instead of the full motion. This in turn implies that conditions of sharp resonance, with accompanying large amplitudes, need not to be covered. But the theory should include consideration to *weakly resonant* motion, i.e., motion influenced but not dominated by resonances in the vicinity of the excitation frequency; otherwise the predictions will be essentially wrong, it will appear. So, first the conditions of strong resonance are determined, and then the response analyzed aside from such conditions.

3.3.1. Resonances

System (1) and its discretized approximation (17) with Eq. (20) possesses both external and parametric resonances. This is seen by introducing new variables $\tilde{v}_i(t) = v_i(t) + g\beta_i/\omega_i^2$, measuring the offset from the static equilibrium $-g\beta_i/\omega_i^2$, by which Eq. (20) becomes

$$\tilde{v}_{itt} + c\tilde{v}_{it} + \omega_i^2\tilde{v}_i + \sum_{j=1}^{n}\gamma_{ij}\tilde{v}_j\Omega a\sin(\Omega t) = \sum_{j=1}^{n} g\gamma_{ij}\beta_j\omega_j^{-2}\Omega a\sin(\Omega t), \quad i = 1, n. \tag{24}$$

The presence of external resonances at $\Omega \approx \omega_i$ readily appears from the action of the harmonic right-hand term on the linear stiffness term of the left side. As for parametric resonances caused by the left-hand excitation term, the analysis of a similar system in Ref. [27] (Section 5.4) can be directly employed. For the present case, where $\gamma_{ij} = \gamma_{ji}$, it turns out that there are parametric combination resonances of the summed type at $\Omega \approx \omega_i + \omega_j, i, j = 1, n$, and that for weak damping c the response is unbounded when $\Omega \in [\Omega_{1i}; \Omega_{2i}]$, where Ω_{1i} is the lower of the following two values:

$$\Omega_{1i,2i} = \frac{(\omega_i + \omega_j)}{(1 \pm \kappa_{ij})} \pm \frac{c^2}{2\kappa_{ij}(\omega_i + \omega_j)} + \mathrm{O}(c^4), \qquad \kappa_{ij} \equiv \frac{a\gamma_{ij}}{2\sqrt{\omega_i\omega_j}}, \quad i = 1, n, \ j = i, n, \tag{25}$$

where the two first terms is a good approximation for weak damping c. At external resonance the response is limited by viscous damping, whereas at parametric resonance the model response grows unbounded, since no limiting non-linearities are included here.

3.3.2. Non-resonant and weakly resonant response

As for the SRP the Galerkin discretized model is considered, i.e., the modal expansion (17) with modal coefficients given by solutions to Eq. (20), which in matrix notation takes the form

$$\mathbf{v}_{tt} + c\mathbf{v}_t + \boldsymbol{\omega}^2\mathbf{v} + \Omega a\boldsymbol{\gamma}\mathbf{v}\sin(\Omega t) = -g\boldsymbol{\beta}, \tag{26}$$

where $\mathbf{v}(t)$ and $\boldsymbol{\beta}$ are n-vectors with components v_i and β_i, respectively, and $\boldsymbol{\gamma}$ and $\boldsymbol{\omega}^2$ are $(n \times n)$ matrices with components γ_{ij} and $\delta_{ij}\omega_i\omega_j$, respectively, where δ_{ij} is Kronecker's delta.

As with the NRP an attempt is made to solve the equations approximately for $\Omega \gg 1$, i.e., again the method of direct separation of motions is used, considering solutions for $\mathbf{v}$ of the form

$$\mathbf{v} = \mathbf{v}_0(t) + \Omega^{-1}\mathbf{v}_1(t, \tau); \qquad \langle \mathbf{v}_1 \rangle = 0, \quad \tau = \Omega t, \tag{27}$$

where $\mathbf{v}_0$ holds the slow components, and $\Omega^{-1}\mathbf{v}_1$ is a rapidly oscillating overlay that has small amplitude and zero fast-time average, and is 2π-periodic in the fast time τ. Inserting this into Eq. (26) and following the same procedure as described for the NRP in Section 3.1, one obtains

the following equations for the slow motions $\mathbf{v_0}$ and the fast motions $\mathbf{v}_1$, respectively:

$$\mathbf{v}_{0tt} + c\mathbf{v}_{0t} + \boldsymbol{\omega}^2\mathbf{v}_0 + a\boldsymbol{\gamma}\langle \mathbf{v}_1 \sin\tau \rangle = -g\boldsymbol{\beta}, \tag{28}$$

$$\begin{aligned}\mathbf{v}_{1\tau\tau} + a\boldsymbol{\gamma}\mathbf{v}_0 \sin\tau + \Omega^{-1}[2\mathbf{v}_{1t\tau} + c\mathbf{v}_{1\tau} + a\boldsymbol{\gamma}(\mathbf{v}_1 \sin\tau - \langle \mathbf{v}_1 \sin\tau \rangle)] \\ + \Omega^{-2}[\mathbf{v}_{1tt} + c\mathbf{v}_{1t} + \boldsymbol{\omega}^2\mathbf{v}_1] = 0.\end{aligned} \tag{29}$$

Even if Ω is supposed to be large, there will typically be one or several elements in $\boldsymbol{\omega}^2$ that is close to Ω or at least of similar order of magnitude. That is, the response to the excitation at most frequencies Ω are significantly affected, though perhaps not dominated, by resonance effects. Then $|\boldsymbol{\omega}^2| = \mathrm{O}(\Omega^2)$ so that $|\Omega^{-2}\boldsymbol{\omega}^2| = \mathrm{O}(1)$, and the last term in the last square bracket of Eq. (29) is comparable in magnitude order to the dominating two first terms. For that case, which is typical for real systems with a high modal density and low damping, Eq. (29) for the fast motions can be written as

$$\mathbf{v}_{1\tau\tau} + \Omega^{-2}\boldsymbol{\omega}^2\mathbf{v}_1 = -a\boldsymbol{\gamma}\mathbf{v}_0 \sin\tau + \mathrm{O}(\Omega^{-1}). \tag{30}$$

To first order this is an undamped and uncoupled set of standard linear single-degree-of-freedom harmonic oscillator equations, with the following stationary solution:

$$\mathbf{v}_1 = a(\mathbf{I} - \Omega^{-2}\boldsymbol{\omega}^2)^{-1}\boldsymbol{\gamma}\mathbf{v}_0 \sin\tau + \mathrm{O}(\Omega^{-1}), \quad \Omega \neq \omega_i, \ \ i = 1, n, \tag{31}$$

where $\mathbf{I}$ is the identity matrix, and the condition that Ω be away from sharp resonance ensures the matrix inverse to be finite. This expression for the fast motions is valid for weakly damped systems at conditions that are not sharply resonant. Finitely small damping and sharp resonance can be accounted for, if needed, by retaining the term $\Omega^{-1}c\mathbf{v}_{1\tau}$ from Eqs. (29) to (30), at the cost of increased complexity of subsequent expressions.

Inserting Eq. (31) into Eq. (28) and evaluating the averaging term, the equation for the slow motions becomes

$$\mathbf{v}_{0tt} + c\mathbf{v}_{0t} + (\boldsymbol{\omega}^2 + \Delta\boldsymbol{\omega}^2)\mathbf{v}_0 = -g\boldsymbol{\beta}, \tag{32}$$

where

$$\Delta\boldsymbol{\omega}^2 \equiv \tfrac{1}{2}a^2\boldsymbol{\gamma}(\mathbf{I} - \Omega^{-2}\boldsymbol{\omega}^2)^{-1}\boldsymbol{\gamma}. \tag{33}$$

Comparing Eq. (32) to Eq. (26), it appears that the equation of slow motions is similar to that of the full motion, though with the rapidly oscillating term replaced by an apparent additional stiffness (per unit mass) $\Delta\boldsymbol{\omega}^2$. Though, since $\Delta\boldsymbol{\omega}^2$ is generally non-diagonal, the n equations of system (32) are coupled, by contrast to the equations for the unexcited system (26).

The stationary solution $\mathbf{v}_0^*$ for the slow motions is obtained by neglecting the time-varying terms and solving for $\mathbf{v}_0$, giving

$$\begin{aligned}\mathbf{v}_0^* &= \lim_{t\to\infty} \mathbf{v}_0(t) = -g(\boldsymbol{\omega}^2 + \Delta\boldsymbol{\omega}^2)^{-1}\boldsymbol{\beta} \\ &= -g(\boldsymbol{\omega}^2 + \tfrac{1}{2}a^2\boldsymbol{\gamma}(\mathbf{I} - \Omega^{-2}\boldsymbol{\omega}^2)^{-1}\boldsymbol{\gamma})^{-1}\boldsymbol{\beta}.\end{aligned} \tag{34}$$

Inserting this and Eqs. (27) and (31) into expansion (17) (rewritten in matrix form, $u = \mathbf{v}^{\mathrm{T}}\boldsymbol{\varphi}$), and averaging the result, it is found that the slow or averaged component of the deflection and the

vibration amplitude is, respectively:

$$\langle u(x,t)\rangle = (\mathbf{v}_0^*)^{\mathrm{T}}\boldsymbol{\varphi}(x),$$
$$\max(u(x,t) - \langle u(x,t)\rangle) = a\Omega^{-1}((\mathbf{I} - \Omega^{-2}\boldsymbol{\omega}^2)^{-1}\boldsymbol{\gamma}\mathbf{v}_0^*)^{\mathrm{T}}\boldsymbol{\varphi}(x) + \mathrm{O}(\Omega^{-2}). \tag{35}$$

Hence the tip lift and the tip amplitude is, respectively,

$$\begin{aligned}\Delta u_0^*(l)_{ARP} &= \langle u(l,t)\rangle^*|_{a\neq 0} - u(l,t)^*|_{a=0} \\ &= g\boldsymbol{\beta}^{\mathrm{T}}((\boldsymbol{\omega}^2)^{-1} - (\boldsymbol{\omega}^2 + \Delta\boldsymbol{\omega}^2)^{-1})\boldsymbol{\varphi}(l),\end{aligned} \tag{36}$$

$$\tilde{u}^*(l)_{ARP} = a\Omega^{-1}((\mathbf{I} - \Omega^{-2}\boldsymbol{\omega}^2)^{-1}\boldsymbol{\gamma}\mathbf{v}_0^*)^{\mathrm{T}}\boldsymbol{\varphi}(l) + \mathrm{O}(\Omega^{-2}), \tag{37}$$

which is valid aside from sharp resonance, i.e., for $\Omega \neq \omega_i$ and $\Omega \notin [\Omega_{1i}; \Omega_{2i}]$, $i = 1, n$.

Results identical to Eqs. (36) and (37) can be obtained by using second order standard averaging, as was shown by Fidlin [28] after this paper was initially submitted. The averaging approach seems more elaborate, but is also better substantiated mathematically.

4. Results: predictions and experiments compared

Here measured frequency and acceleration responses for the experimental string are presented, and compared to theoretical predictions obtained by the NRP, the SRP, and the ARP.

4.1. Frequency response

Fig. 5 shows the tip lift and tip amplitude of the string, in response to HF excitation at fixed acceleration amplitude Ωa and varying frequency Ω, as measured for the experimental string, and as predicted theoretically using the NRP, SRP, and ARP. As appears from Fig. 5(b) the modal density is quite high, with four external resonances (smooth peaks) in this range (f_3–f_6, cf. Table 1), and a number of (sharp-edged) parametric resonances.

The analytical ARP (solid line) and the numerical SRP (dashed) results are almost indistinguishable, except in frequency intervals of parametric resonance, where the ARP expressions (36) and (37) are explicitly not valid. The prediction of these ranges, as given by Eq. (25) and the horizontal arrow lines in Fig. 5(b), matches the SRP results with good accuracy only up to about 130 Hz; for higher frequencies second order approximations (quite lengthy) as given in Ref. [27] may be necessary to improve on the accuracy. The important thing to note is that, aside from sharp resonances, the simple analytical ARP with all its approximations, gives results almost identical to the far more elaborate numerical SRP.

The experimental observations agree quite closely with the ARP (outside sharp resonance) and the SRP. This indicates that the original model (1) captures all essential features for correct quantitative prediction of the phenomenon under study, and also that the approximations involved in using the SRP and in particular the ARP are pertinent.

By contrast the NRP, which assumes no resonant influence at all, provides results in reasonable agreement with experimental results (and thus with the ARP and SRP) only for the very flattest parts of the frequency response. Hence the NRP is useful only for very limited frequency ranges, or for systems having very low modal density or high damping.

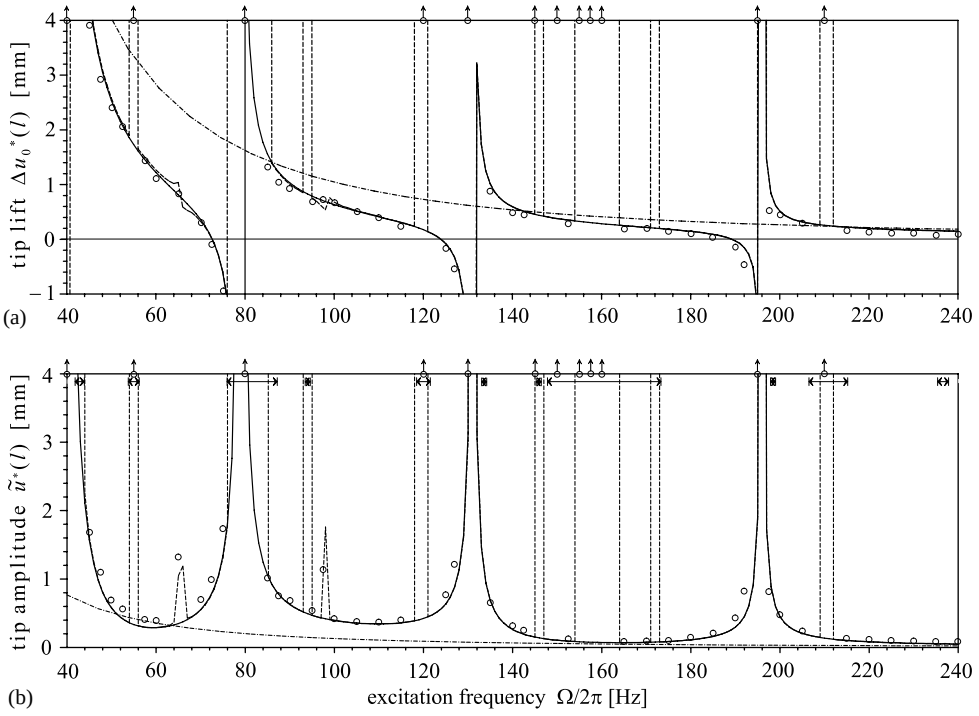

Fig. 5. Frequency response for the $\varnothing 1 \times 550$ mm horizontal string with horizontal base excitation of constant acceleration amplitude $\Omega a = 300\,\mathrm{m/s^2}$, showing (a) vertical tip lift and (b) tip vibration amplitude as a function of input frequency. Circle symbols: experimental measurements (with arrows pointing up indicating large resonant response); lines: theoretical predictions based on the NRP (dash–dotted), the SRP (dashed), and the ARP (solid line); horizontal arrow lines in (b) span parametric resonances predicted by ARP. Parameters: $L = 0.55$, $E = 195 \times 10^9$, $g = 9.82$, $\rho A = 6.1410 \times 10^{-3}$, $EI = 9.5720 \times 10^3$, $\rho Ac = 8 \times 10^{-3}$, $\Omega a = 300$, $n = 6$.

Parametric resonances affect the response within well-defined intervals of Ω, whereas the influence of external resonances disappears only gradually with the distance from resonance. Some of the resonance regions are overlapping, e.g., the external resonance $\Omega \approx f_4 \approx 79\,\mathrm{Hz}$ is within the region ≈ 76–$87\,\mathrm{Hz}$ where the parametric resonance $\Omega \approx 2f_3 \approx 81\,\mathrm{Hz}$ causes unbounded motion. There are also two minor resonance peaks, at 66 and 98 Hz, closely corresponding to $f_5/2 \approx 65.5\,\mathrm{Hz}$ and $f_6/2\,\mathrm{Hz} \approx 98.1\,\mathrm{Hz}$. They occur in the numerical simulation as well as in experiments, but neither resembles parametric nor external resonance—and since they occur for the linear model they are not non-linear (super or subharmonic) resonances. Also note that for excitation frequencies just below the primary external resonances, the tip lift is actually negative, that is: the effective stiffness can also be *lowered* by HF excitation, so that for certain frequencies the tip drops below its unexcited static equilibrium.

4.2. Acceleration response

Fig. 6 shows a set of acceleration responses, i.e., the tip lift as a function of base acceleration, with the frequency kept constant at each of four values corresponding to the flatter parts of the

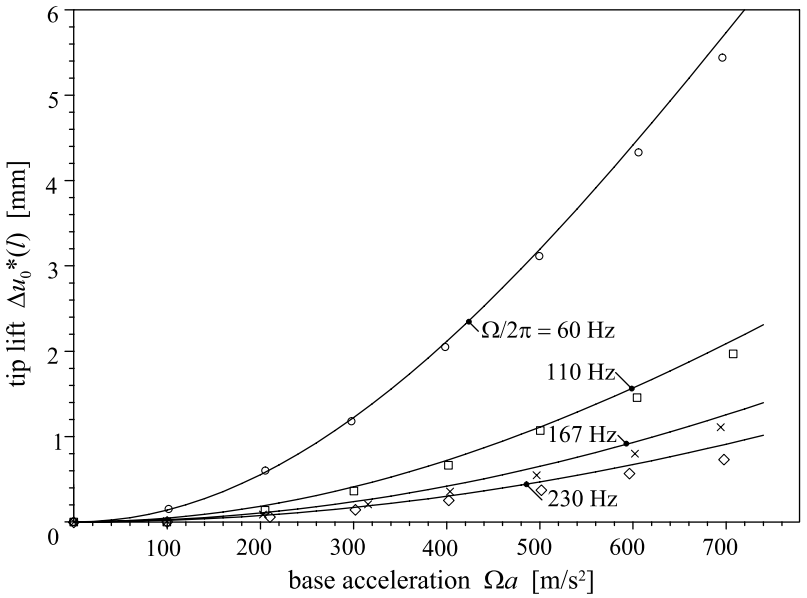

Fig. 6. Tip lift of the string as a function of input acceleration at four different frequencies. Curves: ARP theory; symbol markers: experimental measurements. System parameters as for Fig. 5.

frequency response in Fig. 5. The agreement between ARP theory and experiment is generally good, at least for acceleration levels that are not very high (700 m/s^2 is the maximum capacity of the shaker). The tip lift increases almost quadratically with acceleration, as can be explained by considering the change in stiffness predicted by the ARP: The increase in apparent linear stiffness is $\Delta\boldsymbol{\omega}^2$ (cf. Eq. (32)), which according to Eq. (33) grows with the square of a when resonance effects (second term in parentheses in Eq. (33)) can be neglected. Now $a = \text{acceleration}/\Omega$, where for each curve in Fig. 6 the frequency Ω is kept constant; hence the stiffness and thus the tip lift grows approximately with the square of the acceleration.

4.3. Example closure

In conclusion, the simple ARP provides good predictions for the tip lift and tip amplitude of the experimental string for a wide range of excitation parameters—except at sharp external or parametric resonance, where the theory is explicitly not valid (and not relevant). The SRP gives predictions that are identical to those of the ARP outside sharp resonance, and further gives good predictions at resonance; however this method is purely numerical and thus yields little qualitative insight. The predictions of the NRP does not match those of the ARP and the SRP and the experimental measurements, except at far-from-resonant conditions where the accuracy is fair; however, the ARP does provide some qualitative insight on how the change in apparent stiffness enters into the partial differential equation of motion. Next a generalized class of elastic systems with HF excitation is considered, and ARP used to set up correspondingly general predictions for the change in apparent stiffness.

5. Generalized system and predictions

Consider a class of continuous systems subjected to HF excitation, broad enough to cover many applications of interest, yet sufficiently specific to yield interpretable results:

$$u_{tt} + L_c[u_t] + L_0[u] + \Omega \sum_{k=1}^{N} L_{1k}[u]\sin(m_k \Omega t + \psi_k) = f_0(\mathbf{x}, t) + \Omega f_1(\mathbf{x}, t)\sin(m\Omega t + \psi), \tag{38}$$

where $u = u(\mathbf{x}, t)$ describes a scalar displacement component of a continuous structure at spatial position $\mathbf{x} \in D$ where D is a bounded region, L_c, L_0, and L_{1k} are linear spatial differential operators describing the damping, stiffness, and spatial component of the HF excitation, respectively, $\Omega \gg 1$ is the fundamental excitation frequency, m_k and m are integers, ψ_k and ψ are phasings of the HF excitation, f_0 and f_1 are external distributed forces, with f_0 changing slowly as compared to the base period $2\pi/\Omega$ of the HF excitation, and the term with f_1 containing rapidly fluctuating components. In general, subscript 1 denotes functions and operators related to terms with explicit HF variation, while subscript 0 denotes quantities without such variations. The two HF excitation terms are written with Ω as a factor, to indicate that these are assumed to be "strong". Specifying the HF excitation in terms of harmonic functions implies that the following results will be much more transparent than if generalized time functions were used. Still, quite general time functions can be described for the parametric excitation in Eq. (38), by using the sum to describe a Fourier expansion of the time function. The system description is completed by specifying initial conditions $u(\mathbf{x}, 0)$ and $u_t(\mathbf{x}, 0)$, and linear homogeneous boundary conditions $B_r[u] = 0$, $r = 1, \ldots, 2q$ for $\mathbf{x} \in \partial D_r$, where $\partial D_r \subseteq \partial D$ denotes parts of the boundary of D, q is the order of Eq. (38), and B_r contain spatial derivatives of order 0 through $q - 1$. The extension to the multivariable case can be performed by replacing the scalar functions u, f_0, and f_1 with suitable vectors, and is thus trivial.

The linear eigenvalue problem (e.g., Refs. [3,26,29,30]) associated with the above system is

$$\begin{aligned} L_0[\varphi] &= \omega^2 \varphi, \quad \mathbf{x} \in D, \\ B_r[\varphi] &= 0, \quad \mathbf{x} \in \partial D_r, \end{aligned} \tag{39}$$

which is assumed to be self-adjoint, with eigenvalues ω_i^2 and corresponding normalized eigenvectors $\varphi_i(\mathbf{x})$ satisfying the following orthogonality relations:

$$\int_D \varphi_i \varphi_j \, \mathrm{d}D = \delta_{ij}, \qquad \int_D \varphi_i L_0[\varphi_j] \, \mathrm{d}D = \omega_i^2 \delta_{ij}, \quad i, j = 1, 2, \ldots. \tag{40}$$

The excitation of the system is assumed to be small in displacement amplitude and high in frequency, and the motion u to consist of small, rapidly oscillating components superimposed on slowly changing components. Next approximate equations governing the slow or average components of motion are set up, from which apparent changes in stiffness and related quantities can be predicted.

5.1. The generalized no-resonance prediction (GNRP)

This generalized version of the NRP is useful when Ω is large and far away from any resonances. The main results will be in terms of averaged terms in the original equation of motion, representing the integrated effect of the HF excitation. Repeating the steps described in detail in Section 3.1 for the string system, let

$$u(\mathbf{x},t) = u_0(\mathbf{x},t) + \Omega^{-1}u_1(\mathbf{x},t,\tau), \quad \tau \equiv \Omega t, \tag{41}$$

where u_0 holds the slow motions, and $\Omega^{-1}u_1$ is the rapidly oscillating overlay, 2π-periodic in the fast time τ with a zero fast-time average, $\langle u_1 \rangle = 0$. Then the equation for the slow motions u_0 and the fast motions u_1 becomes, respectively:

$$u_{0tt} + L_c[u_{0t}] + L_0[u_0] + \sum_{k=1}^{N} \langle L_{1k}[u_1]\sin(m_k\tau + \psi_k) \rangle = f_0(\mathbf{x},t), \tag{42}$$

$$u_{1\tau\tau} = -\sum_{k=1}^{N} L_{1k}[u_0]\sin(m_k\tau + \psi_k) + f_1(\mathbf{x},t)\sin(m\tau + \psi) + \mathrm{O}(\Omega^{-1}). \tag{43}$$

A first-order solution for u_1, valid for $\Omega \gg 1$ and neglecting resonance effects, is readily obtained by integrating Eq. (43) (recalling that u_0 does not depend on τ):

$$u_1 = \sum_{k=1}^{N} L_{1k}[u_0]m_k^{-2}\sin(m_k\tau + \psi_k) - f_1(\mathbf{x},t)m^{-2}\sin(m\tau + \psi) + \mathrm{O}(\Omega^{-1}). \tag{44}$$

Inserting this into Eq. (42) and evaluating the averaging term yields the final averaged system:

$$u_{0tt} + L_c[u_{0t}] + \bar{L}_0[u_0] = \bar{f}_0(\mathbf{x},t) + \mathrm{O}(\Omega^{-1}), \tag{45}$$

where

$$\bar{L}_0 \equiv L_0 + \frac{1}{2}\sum_{k,j=1}^{N} m_j^{-2}\delta_{m_k\, m_j}\cos(\psi_k - \psi_j)L_{1k}L_{1j},$$

$$\bar{f}_0 \equiv f_0 - \tfrac{1}{2}m^{-2}\sum_{k=1}^{N} L_{1k}[f_1]\delta_{m_k\, m}\cos(\psi - \psi_k) \tag{46}$$

and where it has been used that $\langle \sin(i\tau + \psi_i)\sin(j\tau + \psi_j) \rangle = \frac{1}{2}\delta_{ij}\cos(\psi_i - \psi_j)$ for $i,j = 1,2,...,$ and it should be recalled that some of the m_k's can be equal.

Thus the effect of the HF excitation, on the average, is to change the stiffness operator L_0, and change the slow external forces f_0. To observers (or measuring instruments) that do not notice (or low-pass filters) the small overlay of HF displacements, it will appear as if the stiffness and the slow forcing has changed. It appears the change in stiffness is independent of the external HF excitation f_1, whereas the change in slow forcing occurs only when external and parametric HF excitation are both present ($f_1 \neq 0$ and $L_1 \neq 0$).

A change in effective stiffness in turn changes related quantities, such as natural frequencies. To find the apparent natural frequencies $\bar{\omega}_i$ in the presence of HF excitation one should solve the eigenvalue problem (39) using $\bar{L}_0$ in place of L_0. Knowing the eigenvalues ω_i^2 and eigenfunctions

φ_i for the unexcited system, an estimate for the change in natural frequencies can be obtained by pre-multiplying the eigenvalue problem $\bar{L}_0\bar{\varphi}_i = \bar{\omega}_i^2\bar{\varphi}_i$ by $\bar{\varphi}_i$, integrate over the domain of the system, assume the change in eigenfunction is negligible, and find

$$\begin{aligned}\bar{\omega}_i^2 &= \int_D \bar{\varphi}_i \bar{L}_0[\bar{\varphi}_i]\,\mathrm{d}D \approx \int_D \varphi_i \bar{L}_0[\varphi_i]\,\mathrm{d}D \\ &= \omega_i^2 + \tfrac{1}{2}\sum_{k,j=1}^{N} m_j^{-2}\delta_{m_k\, m_j}\cos(\psi_k - \psi_j)\int_D \varphi_i L_{1k}L_{1j}[\varphi_i]\,\mathrm{d}D. \end{aligned} \tag{47}$$

Many theorems and methods for continuous systems rely on the self-adjointness of the relevant eigenvalue problems. It appears from the assumed self-adjointness of L_0 and the definition of $\bar{L}_0$ in Eq. (46), that the eigenvalue problem for $\bar{L}_0$ is self-adjoint if $\int_{\mathrm{D}} uL_{1i}L_{1j}[v]\,\mathrm{d}D = \int_{\mathrm{D}} vL_{1i}L_{1j}[u]\,\mathrm{d}D$ for $i,j = 1,2,\ldots$, and for any two test functions $u(\mathbf{x})$ and $v(\mathbf{x})$ satisfying the boundary conditions.

5.2. The GARP

This generalized version of the ARP is useful when Ω is large, and not at sharp external or parametrical resonance with the system; the predictions will be in terms of mode shapes and natural frequencies. Proceeding as described in detail for the string system in Section 3.1, consider the Galerkin discretized model of the general system (38), i.e., let

$$u(\mathbf{x},t) = \mathbf{v}^{\mathrm{T}}(t)\boldsymbol{\varphi}(\mathbf{x}), \tag{48}$$

where the vector $\boldsymbol{\varphi}$ holds the eigenfunctions $\varphi_i(\mathbf{x})$, $i = 1,n$, that are solutions to the eigenvalue problem (39)–(40), and the vector $\mathbf{v} = \mathbf{v}(t)$ holds the modal coefficients v_i, $i = 1,n$, that are solutions to the following linear system of ordinary differential equations:

$$\mathbf{v}_{tt} + \mathbf{c}\mathbf{v}_t + \boldsymbol{\omega}^2\mathbf{v} + \Omega\sum_{k=1}^{N}\boldsymbol{\gamma}_k\mathbf{v}\sin(m_k\Omega t + \psi_k) = \mathbf{p}_0(t) + \Omega\mathbf{p}_1(t)\sin(m\Omega t + \psi), \tag{49}$$

where the components of the matrices $\mathbf{c}$, $\boldsymbol{\omega}^2$, $\boldsymbol{\gamma}_k$, and the vectors $\mathbf{p}_0$, $\mathbf{p}_1$ are, respectively:

$$\begin{aligned} &c_{ij} = \int_D \varphi_j L_c[\varphi_i]\,\mathrm{d}D, \qquad \omega_{ij}^2 = \delta_{ij}\omega_i^2, \qquad \gamma_{k(ij)} = \int_D \varphi_j L_{\,1k}[\varphi_i]\,\mathrm{d}D, \\ &p_{0i}(t) = \int_D f_0(\mathbf{x},t)\varphi_i\,\mathrm{d}D, \qquad p_{1i}(t) = \int_D f_1(\mathbf{x},t)\varphi_i\,\mathrm{d}D, \qquad i,j = 1,n, \quad k = 1,N. \end{aligned} \tag{50}$$

External resonances occur for this system in two cases: (1) when $\mathbf{p}_1 \neq \mathbf{0}$ and $\Omega \approx \omega_i/m$, and (2) when $\mathbf{p}_0$ has a non-zero (long-term) average and $\Omega \approx \omega_i/m_k$, $i = 1,n$, $k = 1,N$.

Parametric resonances also occurs in two cases: (1) when $\gamma_{k(ij)}\gamma_{k(ji)} > 0$ and $\Omega \approx (\omega_i + \omega_j)/m_k$, $i,j = 1,n$, for at least one $k = 1,N$, and (2) when $\gamma_{k(ij)}\gamma_{k(ji)} < 0$ and $\Omega \approx (\omega_i - \omega_j)/m_k$ for at least one k. For vanishing damping, the width of the resonant regions are given by the condition $\gamma_{k(ij)}\gamma_{k(ji)} > \omega_i\omega_j(m_k\Omega - (\omega_i - \omega_j))^2$ in case (1), and by $\gamma_{k(ij)}\gamma_{k(ji)} < -\omega_i\omega_j(m_k\Omega - (\omega_i - \omega_j))^2$ in case (2); see Ref. [27] (Section 5.4) for a detailed treatment of these resonances, and for higher-order approximations and consideration to damping.

To solve Eq. (49) approximately for $\Omega \gg 1$, motions are split into slow and fast components:

$$\mathbf{v} = \mathbf{v}_0(t) + \Omega^{-1}\mathbf{v}_1(t,\tau), \qquad \langle \mathbf{v}_1 \rangle = 0, \quad \tau = \Omega t, \tag{51}$$

where the equations for the slow motions $\mathbf{v}_0$ and the fast motions $\mathbf{v}_1$ becomes, respectively:

$$\mathbf{v}_{0tt} + \mathbf{c}\mathbf{v}_{0t} + \boldsymbol{\omega}^2\mathbf{v}_0 + \sum_{k=1}^{N} \boldsymbol{\gamma}_k \langle \mathbf{v}_1 \sin(m_k\tau + \psi_k)\rangle = \mathbf{p}_0(t), \tag{52}$$

$$\mathbf{v}_{1\tau\tau} + \sum_{k=1}^{N} \boldsymbol{\gamma}_k \mathbf{v}_0 \sin(m_k\tau + \psi_k) - \mathbf{p}_1(t)\sin(m\tau + \psi) + \Omega^{-2}[\mathbf{v}_{1tt} + \mathbf{c}\mathbf{v}_{1t} + \boldsymbol{\omega}^2\mathbf{v}_1] + \Omega^{-1}\left[2\mathbf{v}_{1t\tau} + \mathbf{c}\mathbf{v}_{1\tau} + \sum_{k=1}^{N} \boldsymbol{\gamma}_k(\mathbf{v}_1 \sin(m_k\tau + \psi_k) - \langle \mathbf{v}_1 \sin(m_k\tau + \psi_k)\rangle)\right] = 0. \tag{53}$$

For the case of interest, where resonant effects are significant but not dominating, the term $\Omega^{-2}\boldsymbol{\omega}^2\mathbf{v}_1$ in Eq. (53) is comparable in magnitude to the dominating first terms, so the equation of fast motion can be written as

$$\mathbf{v}_{1\tau\tau} + \Omega^{-2}\boldsymbol{\omega}^2\mathbf{v}_1 = -\sum_{k=1}^{N} \boldsymbol{\gamma}_k \mathbf{v}_0 \sin(m_k\tau + \psi_k) + \mathbf{p}_1(t)\sin(m\tau + \psi) + \mathrm{O}(\Omega^{-1}) \tag{54}$$

with stationary solution (valid when Ω is away from sharp resonance):

$$\mathbf{v}_1 = \sum_{k=1}^{N} (m_k^2\mathbf{I} - \Omega^{-2}\boldsymbol{\omega}^2)^{-1}\boldsymbol{\gamma}_k \mathbf{v}_0 \sin(m_k\tau + \psi_k) - (m^2\mathbf{I} - \Omega^{-2}\boldsymbol{\omega}^2)^{-1}\mathbf{p}_1(t)\sin(m\tau + \psi) + \mathrm{O}(\Omega^{-1}). \tag{55}$$

Inserting into Eq. (52) and evaluating the average, the equation for the slow motions becomes

$$\mathbf{v}_{0tt} + \mathbf{c}\mathbf{v}_{0t} + (\boldsymbol{\omega}^2 + \Delta\boldsymbol{\omega}^2)\mathbf{v}_0 = \mathbf{p}_0(t) + \Delta\mathbf{p}_0(t), \tag{56}$$

where $\Delta\boldsymbol{\omega}^2$ denotes the apparent change in stiffness:

$$\Delta\boldsymbol{\omega}^2 \equiv \tfrac{1}{2}\sum_{k,j=1}^{N} \boldsymbol{\gamma}_k (m_j^2\mathbf{I} - \Omega^{-2}\boldsymbol{\omega}^2)^{-1}\boldsymbol{\gamma}_j \delta_{m_k m_j} \cos(\psi_k - \psi_j) \tag{57}$$

and $\Delta\mathbf{p}_0(t)$ denotes an apparent change in static load:

$$\Delta\mathbf{p}_0(t) \equiv \tfrac{1}{2}\sum_{k=1}^{N} \boldsymbol{\gamma}_k (m^2\mathbf{I} - \Omega^{-2}\boldsymbol{\omega}^2)^{-1}\mathbf{p}_1(t)\delta_{m_k m} \cos(\psi_k - \psi). \tag{58}$$

Expressions (56)–(58) provides straightforward predictions of apparent changes in stiffness and static loading, and facilitates predictions of related quantities such as natural frequencies, buckling loads, and static equilibriums—provided the frequency of excitation Ω is high and not in sharp external or parametric resonance with the system. Below, application of the GNRP and the GARP is illustrated in the form of two brief examples.

5.3. Brief example 1: clamped string with HF base excitation

Reconsider the string problem described in Section 2. The equation of motion (1) for the corresponding beam model is of the general form (38), with $N = 1$, $L_c = c$, $L_0 = \omega_0^2 l^4()_{xxxx}$,

$L_{11} = -a((l—x)()_x)_x$, $m_1 = 1$, $f_0 = -g$, $\psi_1 = f_1 = 0$, and boundary conditions of the required type.

To predict the response under far-from-resonance conditions the GNRP is employed, and Eqs. (45) and (46) used to readily produce the approximation for the equation of slow motions already derived in Section 3.1 using the NRP. This equation provides the basis for prediction of changes in stiffness and related quantities.

Weakly resonant behavior is taking into account by using the GARP expressions (56)–(58) to compute equations governing the slow component of the modal coefficients $\mathbf{v}(t)$; the results becomes those already presented in Section 3.3 using ARP. They can be used directly for predicting apparent changes in stiffness and related quantities, or along with Eq. (48) (with u_0 substituted for u) to predict the slow component $u_0(x,t)$ of the displacement field.

5.4. Brief example 2: square membrane with in-plane HF excitation

Next, the free transverse vibrations of a square membrane, stretched in the (x,y) plane are predicted. The membrane has density ρ and thickness h, and is clamped along the boundary lines $x = 0$ and $y = 0$, while held with tension N_0 per unit length along the two other boundary lines $x = l$ and $y = l$. The arrangement is shaken in the plane, so that points on the clamped boundary lines are translated at high angular frequency Ω along circular paths of small radius $\Omega^{-1}a$, $\Omega \gg 1$, $a = \mathrm{O}(1)$. Assuming small out-of-plane vibrations $u(x,y,t)$, so that in-plane deformations can be ignored, the boundary tension N_0 can be held approximately constant and the equation of transverse motion becomes

$$u_{tt} - ((c_0^2 + (l-x)\Omega a \sin(\Omega t))u_x)_x - ((c_0^2 + (l-x)\Omega a \cos(\Omega t))u_y)_y = 0, \tag{59}$$

where $c_0^2 \equiv N_0/\rho h$ is a squared wave speed, and the boundary conditions are $u(0,y,t) = u(l,y,t) = u(x,0,t) = u(x,l,t) = 0$. This equation is of the general form (38) with $N = 2$, $L_c = 0$, $L_0 = -c_0^2(()_{xx} + ()_{yy})$, $L_{11} = -a((l—x)()_x)_x$, $L_{12} = -a((l—y)()_y)_y$, $m_1 = m_2 = 1$, $\psi_1 = 0$, $\psi_2 = \pi/2$, and $f_0 = f_1 = 0$.

The slow component u_0 of the far-from-resonance response is given by the GNRP, for which application of Eqs. (45)and (46) gives

$$u_{0tt} + \bar{L}_0[u_0] = \mathrm{O}(\Omega^{-1}), \quad \Omega \gg 1, \tag{60}$$

where the effective stiffness operator $\bar{L}_0$ can be written as

$$\begin{aligned} \bar{L}_0 &= L_0 + \tfrac{1}{2}(L_{11}^2 + L_{12}^2) \\ &= -c_0^2(()_{xx} + ()_{yy}) + \tfrac{1}{2}a^2[((l-x)^2()_{xx})_{xx} + ((l-y)^2()_{yy})_{yy}]. \end{aligned} \tag{61}$$

As appears, in the presence of HF excitation ($a \neq 0$) the membrane exhibits bending-like stiffness (fourth order terms) in addition to the stiffness already provided by stretching (second order terms). This in turn implies, e.g., that more boundary conditions are required to solve for u_0, and that travelling waves will appear dispersive instead of non-dispersive.

The GARP is applicable to illustrate how the stiffness might be affected when resonances cannot be ignored, as will typically be the case. For brevity it is assumed here that $0 \ll \omega_1 < \Omega \ll \omega_2$, so that only the first resonance need to be taken into account, and that only the change in ω_1 is to be predicted. Then Eqs. (56)–(58) can be employed with $n = 1$, giving an equation for the slow

component v_0 of the fundamental modal coefficient:

$$v_{0tt} + (\omega_1^2 + \Delta\omega_1^2)v_0 = 0, \qquad \Delta\omega_1^2 \equiv \tfrac{1}{2}(1 - (\omega_1/\Omega)^2)^{-1}(\gamma_1^2 + \gamma_2^2), \tag{62}$$

where $\omega_1 = \sqrt{2}\, c_0\pi/l$ is the fundamental natural frequency for the unexcited membrane, and $\Delta\omega_1$ is the predicted change in this natural frequency due to HF excitation. Using Eq. (50) to calculate $\gamma_{1,2}$, and inserting the normalized fundamental eigenfunction (first solution of $L_0[\varphi] = \omega^2\varphi$ with boundary conditions), $\varphi_1(x, y) = 2l^{-1}\sin(\pi x/l)\sin(\pi y/l)$, one finds $\gamma_1 = \gamma_2 = \pi^2 a/(2l)$ and thus

$$\Delta\omega_1 = (1 - (\omega_1/\Omega)^2)^{-1/2}\left(\frac{\pi^2 a}{2l}\right) \tag{63}$$

which is valid for $0 \ll \omega_1 < \Omega \ll \omega_2$ and Ω away from any parametric resonances. Whether this change is of any practical significance appears to depend on two factors: The relative strength of the HF excitation a/l, and the closeness of Ω to ω_1.

6. Summary and conclusions

A laboratory experiment was set up for demonstrating and measuring the stiffening effect of high-frequency excitation for a clamped–free horizontal string. A mathematical model was proposed for this system, and analyzed using a hierarchy of three approximating theories. One of these (the ARP), proved capable of predicting the vertical string lift due to stiffening in terms of simple expressions, with results agreeing very well with experimental measurements for a wide range of conditions—except at sharp resonance. Since the stiffening effect has no meaning or relevance at sharp resonance anyway, this theory seems the most adequate for typical applications characterized by high modal density and light damping.

Another theory tested (NRP) provides some insight into the stiffening effect of HF excitation, which here shows up in the partial differential equation of motion as an equivalent distributed bending stiffness. However, ignoring all resonant effects, this theory seriously fails in the quantitative prediction of experimental observations, even for excitation frequencies corresponding to the flattest parts of the frequency response in-between resonances. This theory is applicable only for systems with very low modal density or heavy damping.

Thus resonant effects generally needs to be taken into account, as in the ARP and the generalized version GARP, if useful predictions are in need—even if the high-frequency excitation is not close to resonant to the system of concern. The few other studies dealing with high-frequency effects for continuous systems ignore this, and probably therefore fail to produce predictions in quantitative agreement with experiments. Also, the many studies concerning the general response of continuous elastic systems to periodic excitation seem to ignore the (quasi-) static stiffening effect that may occur with strong high-frequency excitation. This present study takes both into account—the stiffening and the resonance effect—to adequately explain a laboratory experiment where they are both manifest.

The string system is believed to be representative, in many respects, of the way other continuous elastic systems may change apparent stiffness in the presence of HF excitation. Thus, with experimental support for the specific system lending confidence to the approach of analysis, expressions for predicting the stiffening effect for a more general class of continuous systems in

linear differential operator form are also provided. An example usage of this is given, predicting the change in natural frequencies for a plane square membrane subjected to plane HF excitation.

Though the stiffening effect might be utilized for technical purposes or devices, it is first and foremost to be considered as a phenomenon that should be taken into account when predicting performance and safety measures such as stiffness, resonance frequencies, and critical loads for structures operating in strongly vibrating environments.

No attempt was made to include consideration to non-linearities for the string system of this study, since good predictive power was achieved with a linear model. For other systems non-linearities may significantly affect the influence of HF excitation, as shown in Ref. [5] for a general class of discrete systems; for example, non-linearities may contribute to raise the apparent linear stiffness. Hence it would be relevant to extent the present general system and analysis with non-linear operator terms (e.g., quadratic or cubic or quite general), and exemplify for specific non-linear systems, e.g., a stretched (rubber) string or plate clamped along the full boundary, and subjected to strong HF excitation.

Acknowledgements

The author would like to thank Dmitri M. Tcherniak, Jakob S. Jensen, Morten H. Hansen, and Alexander Fidlin for inspiring discussions and helpful comments during the course of this work.

References

[1] I.I. Blekhman, Vibrational Mechanics—Nonlinear Dynamic Effects, General Approach Applications, World Scientific, Singapore, 2000.
[2] J.S. Jensen, Non-Trivial Effects of Fast Harmonic Excitation, Ph.D. Thesis, Department of Solid Mechanics, Technical University of Denmark, Lyngby. DCAMM Report, S83.
[3] J.J. Thomsen, Vibrations and Stability, Order and Chaos, McGraw-Hill, London, 1997.
[4] J.J. Thomsen, D.M. Tcherniak, Chelomei's pendulum explained, Proceedings of the Royal Society of London A 457 (2012) (2001) 1889–1913.
[5] J.J. Thomsen, Some general effects of strong high-frequency excitation: stiffening, biasing, and smoothening, Journal of Sound and Vibration 253 (4) (2002) 807–831.
[6] A. Stephenson, On a new type of dynamic stability, Memoirs and Proceedings of the Manchester Literary and Philosophical Society 52 (8) (1908) 1–10.
[7] A. Stephenson, On induced stability, Philosophical Magazine 15 (1908) 233–236.
[8] P. Hirsch, Das pendel mit oszillierendem Aufhängepunkt, Zeitschrift für Angewandte Mathematik und Mechanik 10 (1930) 41–52.
[9] P.L. Kapitza, Dynamic stability of a pendulum with an oscillating point of suspension, Zurnal Eksperimental'noj i Teoreticeskoj Fiziki 21 (5) (1951) 588–597 (in Russian).
[10] A. Feuer, M. Levine, Vibrational control of a flexible beam, International Journal of Control 65 (1996) 803–825.
[11] J.S. Jensen, Non-linear dynamics of the follower-loaded double pendulum with added support-excitation, Journal of Sound and Vibration 215 (1998) 125–142.
[12] D. Acheson, T. Mullin, Ropy magic, New Scientist 157 (2122) (1998) 32–35.
[13] D. Tcherniak, J.J. Thomsen, Slow effects of fast harmonic excitation for elastic structures, Nonlinear Dynamics 17 (1998) 227–246.
[14] J. Galán, W. B. Fraser, D. J. Acheson, A. R. Champneys, The parametrically excited upside-down rod: an elastic jointed pendulum model, Preprint University of Bristol, 2001.

[15] V.N. Chelomei, Mechanical paradoxes caused by vibrations, Soviet Physics Doklady 28 (1983) 387–390.
[16] V.N. Chelomei, On the possibility of increasing the stability of elastic systems by using vibration, Doklady Akademii Nauk SSSR 110 (1956) 345–347 (in Russian).
[17] J.S. Jensen, Buckling of an elastic beam with added high-frequency excitation, International Journal of Non-Linear Mechanics 35 (2000) 217–227.
[18] J.S. Jensen, D.M. Tcherniak, J.J. Thomsen, Stiffening effects of high-frequency excitation: experiments for an axially loaded beam, American Society of Mechanical Engineers, Journal of Applied Mechanics 67 (2000) 397–402.
[19] A.R. Champneys, W.B. Fraser, The 'Indian rope trick' for a parametrically excited flexible rod: linearized analysis, Proceedings of the Royal Society of London A 456 (1995) (2000) 553–570.
[20] W.B. Fraser, A.R. Champneys, The 'Indian rope trick' for a parametrically excited flexible rod; nonlinear and subharmonic analysis, Proceedings of the Royal Society of London A 458 (2002) 1353–1373.
[21] D. Acheson, From Calculus to Chaos: An Introduction to Dynamics, Oxford University Press, Oxford, 1997.
[22] T. Mullin, A. Champneys, W. B. Fraser, J. Galan, D. Acheson, The 'Indian rope trick' via parametric excitation, Proceedings of the Royal Society of London A, to appear.
[23] D.M. Tcherniak, The influence of fast excitation on a continuous system, Journal of Sound and Vibration 227 (1999) 343–360.
[24] M.H. Hansen, Effect of high-frequency excitation on natural frequencies of spinning disks, Journal of Sound and Vibration 234 (2000) 577–589.
[25] M. Zak, Elastic continua in high frequency excitation field, International Journal of Non-Linear Mechanics 19 (1984) 479–487.
[26] W. Flügge, Handbook of Engineering Mechanics, McGraw-Hill, New York, 1962.
[27] A.H. Nayfeh, D.T. Mook, Nonlinear Oscillations, Wiley, New York, 1979.
[28] A. Fidlin, Second order averaging analysis for a system with high-frequency near-resonant excitation, personal communication, 23 November 2001.
[29] L. Meirovitch, Analytical Method in Vibrations, Macmillan, New York, 1967.
[30] D.J. Inman, Vibration, with Control, Measurement and Stability, Prentice-Hall, London, 1989.